Biogeosciences Discuss., 11, 10323–10363, 2014
www.biogeosciences-discuss.net/11/10323/2014/
doi:10.5194/bgd-11-10323-2014

Biogeosciences Discussions
Open Access

On the relationship between ecosystem-scale hyperspectral reflectance and CO_2 exchange in European mountain grasslands

M. Balzarolo[1], L. Vescovo[2,3], A. Hammerle[4], D. Gianelle[2,3], D. Papale[5], and G. Wohlfahrt[4]

[1]PLECO research group, University of Antwerp, Universiteitsplein 1, 2610 Wilrijk, Belgium
[2]Sustainable Agro-Ecosystems and Bioresources Department, Research and Innovation Centre – Fondazione Edmund Mach, Via E. Mach 1, 38010 S. Michele all'Adige, Italy
[3]Foxlab Joint CNR-FEM Initiative, Via E. Mach 1, 38010 S. Michele all'Adige, Italy
[4]Institute of Ecology, University of Innsbruck, Sternwartestr. 15, 6020 Innsbruck, Austria
[5]DIBAF, University of Tuscia, via S. Camillo de Lellis, 01100 Viterbo, Italy

Received: 11 June 2014 – Accepted: 19 June 2014 – Published: 1 July 2014

Correspondence to: M. Balzarolo (manunela.balzarolo@uantwerpen.be)

Published by Copernicus Publications on behalf of the European Geosciences Union.

Abstract

In this paper we explore the use of hyperspectral reflectance measurements and vegetation indices (VIs) derived therefrom in estimating carbon dioxide (CO_2) fluxes (net ecosystem exchange – NEE; gross primary production – GPP), and some key ecophysiological variables related to NEE and GPP (light use efficiency – ε; initial quantum yield – α; and GPP at saturating light – GPP_{max}) for grasslands. Hyperspectral reflectance data (400–1000 nm), CO_2 fluxes and biophysical parameters were measured at three grassland sites located in European mountain regions. The relationships between CO_2 fluxes, ecophysiological variables and VIs derived using all two-band combinations of wavelengths available from the whole hyperspectral data space were analysed. We found that hyperspectral VIs generally explained a large fraction of the variability in the investigated dependent variables and that they generally exhibited more skill in estimating midday and daily average GPP and NEE, as well as GPP_{max}, than α and ε. Relationships between VIs and CO_2 fluxes and ecophysiological parameters were site-specific, likely due to differences in soils, vegetation parameters and environmental conditions. Chlorophyll and water content related VIs (e.g. CI, NPCI, WI), reflecting seasonal changes in biophysical parameters controlling the photosynthesis process, explained the largest fraction of variability in most of the dependent variables. A limitation of the hyperspectral sensors is that their cost is still high and the use laborious. At the eddy covariance with a limited budget and without technical support, we suggest to use at least dual or four channels low cost sensors in the the following spectral regions: 400–420 nm; 500–530 nm; 750–770 nm; 780–800 nm and 880–900 nm. In addition, our findings have major implications for up-scaling terrestrial CO_2 fluxes to larger regions and for remote and proximal sensing sampling and analysis strategies and call for more cross-site synthesis studies linking ground-based spectral reflectance with ecosystem-scale CO_2 fluxes.

1 Introduction

Covering roughly 22 % (80 million ha) of the EU-25 land area, grasslands are among the dominating ecosystem types in Europe (EEA, 2005) and their role in the European carbon balance has received a lot of scientific interest lately (Soussana et al., 2007; Gilmanov et al., 2007; Wohlfahrt et al., 2008; Ciais et al., 2010). While direct measurements of the carbon dioxide (CO_2) exchange, typically made by eddy covariance techniques (Aubinet et al., 2012), have been carried out and are still ongoing at a number of different grassland sites in Europe – notably in the two EU projects GreenGrass (Soussana et al., 2007) and CarboMont (Cernusca et al., 2008) – scaling up these plot-level measurements to the continental scale requires a modelling approach, typically based on or supported by remotely sensed data.

In recent years, SpecNet (http://specnet.info; Gamon et al., 2006), the European COST Action ES0903 (EUROSPEC) (http://cost-es0903.fem-environment.eu/) and the COST Action ES1309 (OPTIMISE; http://www.cost.eu/domains_actions/essem/Actions/ES1309) focused on the use of optical measurement systems as a scale-appropriate means for upscaling plot-scale, and in particular eddy covariance CO_2 flux measurements (Gamon et al., 2010).

Optical remote sensing data are typically cast into the form of so-called vegetation indices (VIs), which make use of the information content of reflected radiation in two or more discrete wavebands and can be, more or less empirically, related to the process of interest.

The typical optical sampling approach, which is linking spectral observations with carbon fluxes, is based on the Monteith equation (1972, 1977):

$$GPP = \varepsilon \times PAR \times fAPAR \quad (1)$$

where ε (light use efficiency; LUE) and fAPAR (fraction of absorbed photosynthetically active radiation) can be retrieved by remote optical observations.

A wide number of VIs that can potentially be used to model grassland productivity (as a proxy of LUE and fAPAR) has been proposed (Gianelle et al., 2009; Wohlfahrt

BGD
11, 10323–10363, 2014

et al., 2010; Rossini et al., 2012). The various VIs differ in their sensitivity to changes in photosynthetic status. "Greeness indices" – such the widely used Normalized Difference Vegetation Index (NDVI) – demonstrated to be a good proxy for fAPAR, but are not sensitive to rapid changes in plant photosynthesis which are induced by common environmental and anthropogenic stressors (Gitelson et al., 2008; Hmimina et al., 2014; Soudani et al., 2014). Such indices have no direct link to photosynthetic efficiency and are rather indicators for the amount of green biomass and thus for canopy structure rather than plant functioning (Gamon et al., 1992; Peñuelas et al., 1995; Hmimina et al., 2014). However, in ecosystems characterized by strong dynamics (e.g. grasslands and crops with a strong green-up and senescence), other VIs are able to effectively monitor seasonal changes in biophysical parameters controlling canopy photosynthesis such as fAPAR and chlorophyll content and, consequently, can be adopted to monitor seasonal and spatial variability of carbon fluxes (Gitelson et al., 2012; Sakowska et al., 2014).

Short-term changes in LUE can be remotely detected through a spectral proxy of the xanthophyll cycle (Photochemical Reflectance Index, PRI; Gamon et al., 1992). The PRI is one of the most promising VIs for a direct estimation of photosynthetic light use efficiency (LUE) and of its seasonal and diurnal variations (Nichol et al., 2002). Latest developments of the sun-induced fluorescence method may allow even more direct remote sensing of plant photosynthesis in the near future (Meroni et al., 2009; Rossini et al., 2010; Frankenberg et al., 2011). At canopy scale, the relationship between PRI and LUE was shown to be site dependent (Garbulsky et al., 2011; Goerner et al., 2011) and strongly affected by environmental conditions (Soudani et al., 2014).

Although the ability to model grassland gross photosynthesis (GPP) based on remote sensing data has increased considerably in the recent years (Gianelle et al., 2009; Wohlfahrt et al., 2010; Rossini et al., 2012; Sakowska et al., 2014), a universal model for GPP estimation applicable across different grasslands and a wide range of environmental conditions has not yet been identified. For instance, Rossini et al. (2012) showed PRI to be a powerful VI in predicting LUE, but this relationship may not always be observed (Gamon et al., 2001; Filella et al., 2004; Rahimzadeh-Bajgiran et al., 2012; Gitelson et al., 2012; Sakowska et al., 2014). Indeed, previous studies usually focussed on single sites with specific characteristics (e.g. climate, vegetation composition, soil type; see Wohlfahrt et al., 2010) and were often based on the use of different sensors, platforms and protocols (Balzarolo et al., 2011), making generalisation difficult. In addition, most of the studies have either relied on reflectance measurements in a few spectral wavebands (e.g. Wohlfahrt et al., 2010 and Sakowska et al., 2014) or a minimum number of bands needed to calculate the most common VIs, missing potentially important information in under-sampled spectral regions that could explain GPP fluxes and variability.

The overarching objective of the present paper is thus to develop a common framework for predicting grassland GPP based on optical remote sensing data. To this end we combine eddy covariance CO_2 flux measurements with ground-based hyperspectral reflectance measurements at three mountain grassland sites in the Austrian and Italian Alps and the Italian Apennines.

2 Materials and methods

2.1 Experimental site description

This study was carried out at three experimental mountain grassland sites in Europe describing different climatic and grassland management range existing in mountain regions of Europe (Table 1).

2.1.1 Amplero

The Amplero site is situated in the Mediterranean Appennine mountains region of Italy (41.90409° N, 13.60516° E) at 884 m a.s.l. This site is characterized by mild, rainy winters and by an intense drought in summer. Amplero is managed as a hay meadow with one cut in late June and extensive grazing during summer and autumn.

2.1.2 Monte Bondone

Monte Bondone site is situated in the Italian Alps (46.01468° N, 11.04583° E) at 1550 m a.s.l. This site is characterized by a typical sub-continental climate with mild summers and precipitation peaks in spring and autumn. Monte Bondone is managed as an extensive meadow with one cut in mid-July.

2.1.3 Neustift

Neustift grassland site is located in the Austrian Alps (47.11620° N, 11.32034° E) at 970 m a.s.l. The climate of this area is continental/Alpine, with precipitation peaks during the summer (July). This site is intensively managed as a hay meadow with three cuts in mid-June, beginning of August and at the end of September.

2.2 Hyperspectral reflectance measurements

As described in Vescovo et al. (2012), canopy hyperspectral reflectance measurements were collected at each site under clear sky conditions around midday (from 10:00 to 14:00 LT) using the same model of a portable spectroradiometer (ASD Hand-Held, Inc., Boulder, CO, USA) at all sites. The spectroradiometer acquires reflectance values between 350 and 1075 nm with a Full Width Half Maximum (FWHM) of 3.5 nm and a spectral resolution of 1 nm. A cosine diffuser foreoptic was used for nadir/zenith measurements. The vegetation irradiance (sensor pointing nadir) and sky irradiance (sensor pointing zenith) were measured by placing the spectroradiometer on a tripod at a height of 1.5 m and by rotating the spectoradiometer alternately to acquire spectra from the vegetation and from the sky. Hemispherical reflectance was derived as the ratio of reflected to incident radiance. Each reflectance spectrum was automatically calculated and stored by the spectroradiometer as an average of 20 readings. Before starting each spectral sampling, a dark current measurement was done. Spectral measurements were collected from spring until the cutting date at Amplero and Monte

Bondone, while at the site in Neustift, which is cut three times during the season, spectral measurements were taken about once per week throughout the growing season of 2006.

2.3 CO_2 flux measurements

Continuous measurements of the net ecosystem CO_2 exchange (NEE) were made by eddy covariance (EC) technique (Baldocchi et al., 1996; Aubinet et al., 2012) at the three sites. In this study we used CO_2 flux data of the years 2005 and 2006 for Monte Bondone and of 2006 for the other sites. Fluxes were calculated starting from high frequency measurements following established protocols (Aubinet et al., 2012). Data gaps due to sensors malfunctioning or violation of the assumptions underlying the EC method were removed and filled using the gap-filling and flux-partitioning techniques as proposed in Wohlfahrt et al. (2008). Ecosystem respiration (Reco) was calculated from the y-intercept of the light response model (see Eq. 4). Gross primary productivity (GPP) was calculated as the difference between NEE and Reco. Half-hourly NEE and GPP values were averaged around midday (10:00–14:00 LT), to allow for direct comparison with the hyperspectral data, and daily sums were also computed.

2.4 Estimation of grassland ecophysiological parameters

Canopy light use efficiency (ε) was derived from photosynthetically active radiation (PAR) absorbed by the canopy (APAR) as:

$$\varepsilon = \frac{\mathrm{GPP}}{\mathrm{APAR}} = \frac{\mathrm{GPP}}{\mathrm{PAR} \times \mathrm{fAPAR}} \tag{2}$$

and it was estimated both at midday and daily time resolution. We estimated the fraction of PAR absorbed by the canopy (fAPAR) from measured values of the leaf area index (LAI) using the Lambert–Beer law:

$$\mathrm{fAPAR} = 0.95\left(1 - e^{(-k\,\mathrm{LAI})}\right) \tag{3}$$

BGD
11, 10323–10363, 2014

where k is the canopy extinction coefficient (fixed at $k = 0.4$; Kiniry et al., 2007) and 0.95 is the proportion of intercepted PAR that is absorbed by plants (Schwalm et al., 2006). LAI was quantified non-destructively by an indirect method based on canopy PAR transmission using line PAR sensors (SunScan, Delta-T, UK) and inversion of a radiative transfer model (Wohlfahrt et al., 2001). These measurements were done within the footprint area of the spectroradiometer simultaneously with the hyperspectral measurements.

Three additional key parameters of the response of NEE to PAR were extracted by fitting measured NEE and PAR to a simple Michaelis–Menten-type model:

$$\mathrm{NEE} = \frac{-\alpha \mathrm{PAR} F_{\mathrm{sat}}}{\alpha \mathrm{PAR} + F_{\mathrm{sat}}} + R_{\mathrm{eco}} \tag{4}$$

where α represents the apparent quantum yield (µmol CO_2 µmol photons^{-1}), F_{sat} the asymptotic value of GPP (µmol CO_2 m^{-2} s^{-1}), PAR the photosynthetically active radiation (µmol photons m^{-2} s^{-1}) and R_{eco} the ecosystem respiration (µmol CO_2 m^{-2} s^{-1}). Using the Levenberg–Marquardt algorithm the parameters of Eq. (4) were estimated by fitting Eq. (4) to the data, which were pooled into 3 day blocks centered on the date of the hyperspectral data acquisition. For each acquisition date, we then used Eq. (3) to derive GPP at an incident PAR of 1500 µmol m^{-2} s^{-1}, referred to as GPP_{max} in the following.

2.5 Hyperspectral data analysis

In order to explore the information content of the hyperspectral data for estimating CO_2 fluxes (i.e. midday/daily average of NEE and GPP) and ecophysiological parameters (i.e. α, ε and GPP_{max}), we performed a correlation analysis between spectral reflectance indices (independent variables) and these (dependent) variables. To this end, we derived spectral ratio (SR; Eq. 5), spectral difference (SD; Eq. 6) and normalized spectral difference (NSD; Eq. 6) indices using all possible two-band (i and j) reflectance (ρ) combinations between 400 and 1000 nm (180 600 combinations). These three formulations were selected since they represent the most common equations used to compute vegetation indices (see Table 2).

$$\mathrm{SR}_{i,j} = \frac{\rho_i}{\rho_j} \tag{5}$$

$$\mathrm{SD}_{i,j} = \rho_i - \rho_j \tag{6}$$

$$\mathrm{NSD}_{i,j} = \frac{\rho_i - \rho_j}{\rho_i + \rho_j} \tag{7}$$

Linear and exponential regression analyses were performed among all possible wavelength-combinations for all three index-types (SR, NSD and SD) and the investigated dependent variables.

The performances of linear and exponential models in predicting dependent variables (i.e. carbon fluxes and ecophysiological parameters) were evaluated by coefficients of determination (R^2) and root mean square error (RMSE):

$$R^2 = \left(\frac{\sum_{i=1}^{N} \left(P_i - \overline{P}\right)\left(O_i - \overline{O}\right)}{\sqrt{\sum_{i=1}^{N} \left(P_i - \overline{P}\right)^2 \sum_{i=1}^{N} \left(O_i - \overline{O}\right)^2}} \right)^2 \tag{8}$$

$$\mathrm{RMSE} = \sqrt{\frac{1}{N} \sum_{i=1}^{N} (P_i - O_i)^2} \tag{9}$$

where O_i is midday/daily averaged measured fluxes and P_i the midday/daily simulated fluxes; $\overline{O}$ and $\overline{P}$ denote the respective means.

The coefficients of determination (R^2) resulting from the linear and exponential models were visualized in correlograms as depicted in an exemplary fashion in Fig. 1. For clarity we have decided to show in the text only the highest 10 % of the R^2 values with a p value smaller than 0.05 and mask all other values and added a symbol (asterisk) indicating the two-band combination with the highest R^2 value to each correlogram (Fig. 1). The unmasked correlograms are shown in the Supplement for reference.

We also calculated four SR- and seven NSD-indices which are commonly used in relation to vegetation activity and CO_2 fluxes (Table 2). Figure 1 shows also the location of these indices in the waveband space of the correlograms. In this analysis, we also considered the Enhanced Vegetation Index (EVI), which is one of the most frequently used vegetation index to predict CO_2 fluxes. In the Fig. 1 the location of EVI is not shown since this index is computed by the combination of three spectral bands as shown in Table 2.

To select the most appropriate model (i.e. linear or exponential) for predicting grassland CO_2 fluxes and ecophysiological parameters the Akaike information criterion (AIC, Akaike, 1973) was used:

$$\mathrm{AIC} = n \log(\mathrm{Res}) + 2p \tag{10}$$

where n is the number of observations, p is the number of fitted parameters plus one, and Res is the residual sum of squares divided by n. The model with the lowest AIC represents the best model.

3 Results

3.1 Seasonal variation of meteorological variables, LAI and CO_2 fluxes

Environmental conditions and the seasonal development of LAI, NEE, GPP, α, ε and GPP_{max} during the study period are shown in Fig. 2. A strong influence of the typical climatic conditions at the three study sites is evident: Amplero was characterized by a Mediterranean climate, with highest incoming radiation and temperatures, and the lowest amount of precipitation which translated into a substantial seasonal drawdown

BGD
11, 10323–10363, 2014

of soil moisture; Monte Bondone and Neustift, more influenced by continental Alpine climate, experienced comparably lower temperatures with higher precipitation and soil moisture with respect to Amplero (Fig. 2).

Maximum LAI values were similar at Monte Bondone and Amplero (2.8–3.4 $m^2\ m^{-2}$), while, twice as much leaf area developed at the more intensively managed study site Neustift, which was also characterized by higher NEE and GPP (i.e. more photosynthesis and net uptake of CO_2). The reductions in leaf area associated with the cuts of the grasslands were associated as expected with marked increases and reductions in NEE and GPP, respectively. The canopy light use efficiency, ε, was inversely related to GPP and LAI, peaking at the beginning of the season at Amplero and Monte Bondone (0.002–0.020 µmol photons µmol CO_2^{-1}), while for Neustift ε showed the highest values after the cuts (0.015–0.020 µmol photons µmol CO_2^{-1}). At Amplero, α and GPP_{max} peaked in spring and then decreased during the summer drought period, while at Neustift and Monte Bondone, temporal patterns of α and GPP_{max} were more strongly affected by management.

3.2 Hyperspectral data and their relation to CO_2 fluxes and ecophysiological parameters

Figure 3 reports key spectral signatures of the grasslands collected during the study period. The reflectances in the NIR region decreased (NIR; 700–1000 nm) and increased in the blue region (420–540 nm) from early to late spring until the harvest for the Mediterranean grassland of Amplero (Fig. 3a) (Balzarolo, 2008). This is a typical trend for Mediterranean grasslands characterized by leaf senescence due to drought conditions (Fava et al., 2007; Vescovo et al., 2012). For Monte Bondone and Neustift (Fig. 3b–d), the reflectance in the green (540–580 nm) and NIR region increased and decreased in the blue region with increasing LAI and phytomass.

Figures 4–6 show correlograms between NSD-, SR- and SD-type indices, respectively, and the investigated dependent CO_2 flux metrics using a linear model. Figures 6, 7 and 9 show the same analysis, but for the exponential model. Only 10 % of the band combinations with the highest R^2 values are shown for clarity, the unmasked correlograms can be found in the Supplement. A number of interesting insights may be gained from Figs. 4–9, and their counterparts shown in the Supplement, which we summarize in the following:

(i) The correlograms exhibited quite different patterns – some correlograms showed that a wide range of band combinations was able to explain the simulated quantities (e.g. α at Neustift; Fig. S1), while some correlograms exhibited pronounced patterns, with the R^2 value changing greatly with subtle changes in band combinations (e.g. GPP_{max} at Neustift; Fig. S1).

(ii) Maximum R^2 values were often clearly higher than the surrounding areas of high predictive power (e.g. ε at Amplero; Fig. 4).

(iii) The different types of indices (compare Figs. 4–6 or Figs. 5–7) yielded similarly high correlations with the same dependent variable at the same site in similar spectral regions, indicating that band selection is more important for explanatory power than the mathematical formulation of the VI (i.e. ratio vs. difference, with/without normalization). SR and NSD indices (Figs. 4 and 5 or Figs. 7 and 8) yielded similar results compared to SD indices (Fig. 6 or Fig. 9).

(iv) Large differences existed between the study sites in the explanatory power of the same index for the same dependent variable. The highest R^2 values were generally obtained for Amplero, followed by Neustift and then Monte Bondone and the lowest R^2 values resulted when data from all three sites were pooled, confirming the difficulties in finding a general relation valid among sites. Overall, the maximum R^2 values were significant for all individual sites and all sites pooled for all dependent variables and the three types of indices. For all sites pooled, maximum R^2 values ranged between 0.36–0.52 for the linear models (Figs. 4–6) and between 0.40–0.59 for the exponential models (Figs. 7–9).

BGD
11, 10323–10363, 2014

(v) Across all sites and indices, the highest correlations were typically observed for GPP_{max}, while the lowest correlations resulted for α and ε.

(vi) The highest correlations for all dependent variables were found either for indices combining bands in the visible range (< 700 nm) or the red edge and NIR (> 700 nm), corresponding to spectral regions used by indices such as the SRPI, NPCI, PRI and NPQI and the CI and WI, respectively. Spectral regions of well-known indices, such as NDVI, SR, EVI, SIPI or GRI, which exploit the contrasting reflectance magnitudes in the visible and NIR (Fig. 3), resulted in comparably lower correlations.

(vii) Generally, the exponential and linear regression models showed high correlations with the same dependent variable at the same site in similar spectral regions (e.g. GPP_{max} at Neustift; Figs. 4 and 7). Large differences existed between exponential and linear model in explaining the variability of GPP and NEE for Amplero and ε for Monte Bondone. Across all sites, exponential and linear regression model showed similar R^2 variability for all predicting variables except for ε and the exponential regression model showed the highest R^2.

Figure 10 shows the differences between AIC obtained for the linear and exponential models between NSD-type indices and midday average carbon fluxes, and ecophysiological variables. The red area shows waveband combinations where the linear models performed better than the exponential ones (i.e. AIC for linear model was smaller than AIC for exponential model), while the blue area represents the reverse. The same analysis was done also for the SR- and SD-type indices and the results can be found in the Supplement (Figs. S10 and S11).

Figure 10 shows that the exponential model was superior to the linear model for predicting midday GPP, ε and NEE for Amplero and ε for Monte Bondone for all NSD-type indices. For the others variables and sites a clear distinction between the performance of linear and exponential models could be observed. For example, the exponential

BGD
11, 10323–10363, 2014

model best explained GPP_{max} for Neustift in the water band combinations. Similar results were obtained for SR-type indices (Fig. S10). Large differences were also observed for SD-type indices for ε at Neustift (Fig. S11).

Figures S12–S14 in the Supplement display the results of the AIC test for daily GPP, ε and NEE and NSD-, SR- and SD-type indices. The AIC test showed the same results as for midday predictions for ε for all sites and indices. Large differences were apparent for GPP and NEE for Amplero and for GPP for Neustift in the water band combinations.

3.3 Correlation between conventional VIs, ecophysiological variables and CO_2 fluxes

The correlation analysis between the conventional VIs, the CO_2 fluxes (Table 3) and ecophysiological parameters (Table 4), generally confirmed the results obtained with the hyperspectral data.

For the same dependent variable (α, GPP_{max}, GPP, ε and NEE), the performance of the various VIs showed wide differences between sites. For example, for GPP_{max} all of the investigated indices except NPQI resulted in significant linear and exponential correlations at Amplero and Monte Bondone, explaining 30–93 % of the variability in GPP_{max}. In contrast, only PRI, NPCI and SRPI showed a significant linear and exponential performance (30–40 % explained variability) for GPP_{max} at Neustift.

The different VIs performed differently in predicting the same dependent variable at the different study sites. For all dependent variables (Tables 3, 4 and S1), the VI resulting in the highest R^2 values was never the same at all sites. Often the best fitting VI at one site resulted in a non-significant correlation at another site. Therefore, none of the dependent variables clearly emerged as the one best predicted (Tables 3, 4 and S1). The linear and exponential models generally correlated well for the same dependent variables for the same site. The exponential model showed highest R^2 values and the lowest RMSE values. Moreover, the exponential model showed the lowest AIC value.

When data from all sites were pooled, linear and exponential models showed the same performance for the same VI and dependent variable except for GPP and NEE.

BGD
11, 10323–10363, 2014

The best performing VIs for GPP was PRI for the linear model and SIPI for the exponential model; for NEE CI for the linear model and SIPI for the exponential model. NPQI performed best for α, GRI for ε, SIPI for GPP_{max}.

The choice of the averaging period (midday vs. daily) applied to ε, NEE and GPP did generally not modify the ranking of the VIs, but the R^2 values tended to be similar or somewhat higher at the daily time scale (compare Tables 3 and 4 with Table S1). Moreover, AIC values at the daily time scale tended to be lower than at the midday time scale.

4 Discussion

This study aimed at evaluating the potential of hyperspectral reflectance measurements to simulate CO_2 fluxes and ecophysiological variables of European mountain grasslands over a range of climatic conditions and management practices (grazing, harvest). To this end, we combined eddy covariance CO_2 flux measurements with ground-based hyperspectral measurements at three mountain grassland sites in Europe.

The first main result of our study is that, despite focusing on a single type of ecosystem, large differences existed among the investigated sites in the relationships between hyperspectral reflectance data and CO_2 fluxes and ecophysiological parameters. As mentioned by Wohlfahrt et al. (2010), this indicates that site-specific factors not taken into account in the present analysis apparently play a major role in shaping the observed relationships (see also Soudani et al., 2014). For all study sites pooled, hyperspectral reflectance data explained 36–52 % of the variability in the dependent variables for the linear models and 40–59 % for the exponential models. The conventional VIs explained 26–32 % of the variability for the linear models and 29–48 % for the exponential models. In addition, the exponential model performed better than the linear model by showing generally lower AIC values. These findings challenge the current practice in up-scaling to larger regions by grouping all grasslands into a single plant functional type (PFT). We advocate more studies to be conducted merging

CO_2 flux with hyperspectral data by means of models which use a more process-oriented and coupled approach to simulating canopy CO_2 exchange and reflectance in order to explore the causes underlying the observed differences between seemingly closely related study sites. These findings also suggest that waveband combinations not exploited by presently used (conventional) VIs may offer potential for predicting grassland CO_2 fluxes, which has implications for the design and capabilities of future space/airborne or ground-based low cost sensors.

The second relevant result of this study is that the largest fraction of variability in CO_2 fluxes and ecophysiological parameters was explained by band combinations in either the visible region (which is sensitive to pigment absorption) or the NIR region (which is sensitive to canopy structure or water content; Vescovo et al., 2012). In the second case, the correlograms clearly indicate that band combinations between 750 nm and 900 nm (i.e. NIR shoulder region) performed very well for predicting GPP and NEE both for single sites and all sites pooled. In addition, for hyperspectral band combinations including a band which is < 760 nm, the correlation was related to chlorophyll content (Hatfield at al., 2008; Clevers and Gitelson, 2013), while for band combinations > 760 nm (e.g. 761 and 770, 761 and 850, 800 and 850, etc.) there was perhaps a structural effect. These results indicate that the region of near-uniform reflectance throughout the NIR shoulder in ecosystems characterized by strong dynamics can provide useful information on canopy structure and biophysical parameters related to photosynthesis such as fAPAR and, thus, on GPP and NEE.

Over all sites, VIs related to chlorophyll content (e.g. CI and NPCI) (Table 2) emerged as the VIs which explained the largest fraction of variability in most of the dependent variables for the comparably well-watered sites Neustift and Monte Bondone. SR and WI performed well for Amplero, a Mediterranean mountain grassland characterized by a pronounced summer drought (Tables 3 and 4). PRI showed the best performance in predicting α for Amplero and midday GPP for all sites pooled. In addition PRI showed good performance in predicting midday and daily ε for Amplero. VIs such as the NDVI are related to changes in LAI and biomass (Gianelle et al., 2009; Vescovo et al., 2012),

BGD
11, 10323–10363, 2014

but are not able to track changes of the photosynthetic efficiency (with constant LAI) over short time scales (e.g. a few days) (Soudani et al., 2014). The leaf water status influences the photosynthetic efficiency (α and ε) and therefore reflectance at 970 nm, related to leaf water content, and the related WI index may be a good proxy for these parameters (Inoue et al., 2008). In addition, these indices are not sensitive to short term stresses, such as water stress (Gitelson et al., 2008).

The third result of this study is that hyperspectral data and VIs derived therefrom were more successful in predicting GPP_{max}, derived from light response curves, as well as midday and daily average GPP and NEE, while less of the variability was explained in α and ε. This result is somewhat astonishing as variations in absorbed PAR are thought to present a major factor modulating GPP and NEE in mountain grasslands (Wohlfahrt et al., 2008) and form the basis for the concept of light use efficiency (LUE) models. However, this is the first study comparing different grasslands characterized by different plant species and environmental conditions. The use of simple models based on a linear relationship between GPP and VIs, related to canopy greenness, has proven be a good proxy for GPP of ecosystems with strong green-up and senescence (Peng et al., 2011; Rossini et al., 2012). The loss of this relationship may be related to low LUE variability due to abiotic and biotic stressors, the dependency of PRI on LAI, leaf and canopy biochemical structure (e.g. leaf orientation), and xanthophyll cycle inhibition or saturation and zeaxanthin-independent quenching (Gamon et al., 2001; Filella et al., 2004; Rahimzadeh-Bajgiran et al., 2012; Hmimina et al., 2014). For alpine grasslands, a key meteorological variable that played a relevant role in stimulating LUE was high soil water content associated with low temperatures (Polley et al., 2011). Low soil water contents triggered a decrease in leaf conductance as well as in ε and in α also for two oak and beech ecosystems (Hmimina et al., 2014). However, no significant differences in leaf biochemical and structural properties of the canopy at lowest and highest water content were found. In addition, in this special issue, Sakowska et al. (2014) show that ε is also strongly affected by the directional distribution of incident PAR, i.e. the ratio of direct to diffuse PAR. Nevertheless, all these aspects are presently not considered in most LUE models. For instance, the MOD17 algorithm used for the MODIS GPP product (Heinsch et al., 2006) is based on air temperature, vapor pressure deficit, PAR and fAPAR.

5 Conclusions

The present study focused on understanding the potential of hyperspectral VIs in predicting grassland CO_2 exchange and ecophysiological parameters (α, ε and GPP_{max}) for different European mountain grasslands.

The major finding of this study is that the relationship between ground-based hyperspectral reflectance and the ecosystem-scale CO_2 exchange of mountain grasslands is much more variable than what might be supposed given this closely related group of structurally and functionally similar ecosystems. As a consequence, the unique models of mountain grassland CO_2 exchange, i.e. the best fitting models for all sites pooled, explained < 30 % and < 50 % of the variability in the independent variables when established VIs and optimized hyperspectral VIs, respectively, were used. Interestingly, VIs based on reflectance either in the visible or NIR part of the electromagnetic spectrum were superior in predicting mountain grassland CO_2 exchange and ecophysiological parameters compared to commonly used VIs which are based on a combination of these two wavebands. Although the hyperspectral sensors give the possibility to use full spectral information and to compute any desired VIs, their cost is still high. Therefore, at the eddy covariance with a limited budget we suggest to use at least dual or four channels low cost sensors in the the following spectral regions: 400–420 nm; 500–530 nm; 750–770 nm; 780–800 nm and 880–900 nm.

The take-home message from this study thus is that continuing efforts are required to better understand differences in the relationship between ecosystem-scale reflectance and CO_2 exchange and to improve models of this relationship which can be employed to up-scale the land CO_2 exchange to larger spatial scales based on optical remote sensing data. Initiatives such as SpecNet (http://specnet.info; Gamon et al., 2006),

Discussion Paper | Discussion Paper | Discussion Paper | Discussion Paper |

BGD

11, 10323–10363, 2014

the COST Action ES0903 (EUROSPEC; http://cost-es0903.fem-environment.eu/) and the COST Action ES1309 (OPTIMISE; http://www.cost.eu/domains_actions/essem/Actions/ES1309) are instrumental to this end as they provided the scale-consistent combination of hyperspectral reflectance and CO_2 exchange data.

The Supplement related to this article is available online at doi:10.5194/bgd-11-10323-2014-supplement.

Acknowledgements. M. Balzarolo acknowledges the support by the Methusalem program of the Flemish Government. L. Vescovo and D. Gianelle acknowledge the financial support obtained by the EU project CARBOEUROPE-IP (GOCE-CT-2003-505572) and the CARBOITALY project funded by the Italian Government. G. Wohlfahrt and A. Hammerle acknowledge financial support by the Austrian National Science Fund (FWF) through grant agreements P17562 and P26425 and the Tyrolean Science Fund through grant agreement UNI-404/33. A. Hammerle was financially supported through a DOC fellowship by the Austrian Academy of Sciences (ÖAW).

EUROPEAN COOPERATION IN SCIENCE AND TECHNOLOGY

This publication is supported by COST – www.cost.eu

References

Akaike, H.: Information theory and an extension of the maximum likelihood principle, in: Proceedings of the Second International Symposium on Information Theory, edited by: Petrov, B. N. and Csaki, F., Akademiai Kiado, Budapest, 267–281 (Reproduced in: Breakthroughs in Statistics, edited by: Kotz, S. and Johnson, N. L., 2003), Vol. I, Foundations and Basic Theory, Springer-Verlag, New York, 610–624, 1973.

Aubinet, M., Vesala, T., and Papale, D.: Eddy Covariance – a Practical Guide to Measurement and Data Analysis, Springer, 2012.

Baldocchi, D., Valentini, R., Running, S., Oechel, W., and Dahlman, R.: Strategies for measuring and modelling carbon dioxide and water vapour fluxes over terrestrial ecosystems, Glob. Change Biol., 2, 159–168, 1996.

Balzarolo, M.: Biometric Parameters and Fluxes Estimations in Mediterranean Mountainous Grassland with Remote Sensing Techniques, Ph.D. thesis, University of Tuscia, 2008.

Balzarolo, M., Anderson, K., Nichol, C., Rossini, M., Vescovo, L., Arriga, N., Wohlfahrt, G., Calvet, J.-C., Carrara, A., Cerasoli, S., Cogliati, S., Daumard, F., Eklundh, L., Elbers, J. A., Evrendilek, F., Handcock, R. N., Kaduk, J., Klumpp, K., Longdoz, B., Matteucci, G., Meroni, M., Montagnani, L., Ourcival, J.-M., Sanchez-Canete, E. P., Pontailler, J.-Y., Juszczak, R., Scholes, B., and Pilar Martin, M.: Ground-based optical measurements at European flux sites: a review of methods, instruments and current controversies, Sensors, 11, 7954–7981, 2011.

Barnes, J. D., Balaguer, L., Manrique, E., Elvira, S., and Davison, A. W.: A reappraisal of the use of DMSO for the extraction and determination of chlorophylls a and b in lichens and higher plants, Environ. Exp. Bot., 32, 85–100, 1992.

Cernusca, A., Bahn, M., Berninger, F., Tappeiner, U., and Wohlfahrt, G.: Effects of land-use changes on sources, sinks and fluxes of carbon in European mountain grasslands, Ecosystems, 11, 1335–1337, 2008.

Ciais, P., Wattenbach, M., Vuichard, N., Smith, P., Piao, S. L., Don, A., Luyssaert, S., Janssens, I. A., Bondeau, A., Dechow, R., Leip, A., Smith, P. C., Beer, C., van der Werf, G. R., Gervois, S., Van Oost, K., Tomelleri, E., Freibauer, A., Schulze, E. D., and Team, C. S.: The european carbon balance, Part 2: Croplands, Glob. Change Biol., 16, 1409–1428, 2010.

Clevers, J. G. P. W. and Gitelson, A. A.: Remote estimation of crop and grass chlorophyll and nitrogen content using red-edge bands on Sentinel-2 and -3, Int. J. Appl. Earth Obs., 23, 344–351, doi:10.1016/j.jag.2012.10.008, 2013.

EEA: Agriculture and Environment in EU-15, The IRENA Indicator Report, EEA, Copenhagen, 2005.

Fava, F., Colombo, R., Bocchi, S., Meroni, M., Sitzia, M., Fois, N., and Zucca, C.: Identification of hyperspectral vegetation indices for Mediterranean pasture characterization, Int. J. Appl. Earth Obs., 11, 233–243, 2009.

Filella, I., Peñuelas, J., Llorens, L., and Estiarte, M.: Reflectance assessment of seasonal and annual changes in biomass and CO_2 uptake of a Mediterranean shrubland submitted to experimental warming and drought, Remote Sens. Environ., 90, 308–318, 2004.

Frankenberg, C., Fisher, J. B., Worden, J., Badgley, G., Saatchi, S. S., Lee, J.-E., Toon, G. C., Butz, A., Jung, M., Kuze, A., and Yokota, T.: New global observations of the terrestrial carbon cycle from GOSAT: patterns of plant fluorescence with gross primary productivity, Geophys. Res. Lett., 38, L17706, doi:10.1029/2011gl048738, 2011.

Gamon, J. A., Peñuelas, J., and Field, C. B.: A narrow-waveband spectral index that tracks diurnal changes in photosynthetic efficiency, Remote Sens. Environ., 41, 35–44, 1992.

Gamon, J. A., Field, C. B., Fredeen, A. L., and Thayer, S.: Assessing photosynthetic downregulation in sunflower stands with an optically-based model, Plant Biology, 67, 113–125, 2001.

Gamon, J. A., Rahman, A. F., Dungan, J. L., Schildhauer, M., and Huemmrich, K. F.: Spectral Network (SpecNet): What is it and why do we need it?, Remote Sens. Environ., 103, 227–235, 2006.

Gamon, J. A., Coburn, C., Flanagan, L. B., Huemmrich, K. F., Kiddle, C., Sanchez-Azofeifa, G. A., Thayer, D. R., Vescovo, L., Gianelle, D., Sims, D. A., Rahman, A. F., and Pastorello, G. Z.: SpecNet revisited: bridging flux and remote sensing communities, Can. J. Remote Sens., 36, S376–S390, 2010.

Garbulsky, M. F., Peñuelas, J., Gamon, J., Inoue, Y., and Filella, I.: The photochemical reflectance index (PRI) and the remote sensing of leaf, canopy and ecosystem radiation use efficiencies – a review and meta-analysis, Remote Sens. Environ., 115, 281–297, 2011.

Gianelle, D., Vescovo, L., Marcolla, B., Manca, G., and Cescatti, A.: Ecosystem carbon fluxes and canopy spectral reflectance of a mountain meadow, Int. J. Remote Sens., 30, 435–449, 2009.

Gilmanov, T. G., Soussana, J. F., Aires, L., Allard, V., Ammann, C., Balzarolo, M., Barcza, Z., Bernhofer, C., Campbell, C. L., Cernusca, A., Cescatti, A., Clifton-Brown, J., Dirks, B. O. M., Dore, S., Eugster, W., Fuhrer, J., Gimeno, C., Gruenwald, T., Haszpra, L., Hensen, A., Ibrom, A., Jacobs, A. F. G., Jones, M. B., Lanigan, G., Laurila, T., Lohila, A., Manca, G., Marcolla, B., Nagy, Z., Pilegaard, K., Pinter, K., Pio, C., Raschi, A., Rogiers, N., Sanz, M. J., Stefani, P., Sutton, M., Tuba, Z., Valentini, R., Williams, M. L., and Wohlfahrt, G.: Partitioning European grassland net ecosystem CO_2 exchange into gross primary productivity and ecosystem respiration using light response function analysis, Agr. Ecosyst. Environ., 121, 93–120, 2007.

Gitelson, A. A. and Merzlyak, M. N.: Remote estimation of chlorophyll content in higher plant leaves, Int. J. Remote Sens., 18, 2691–2697, 1997.

Gitelson, A. A., Vina, A., Masek, J. G., Verma, S. B., and Suyker, A. E.: Synoptic monitoring of gross primary productivity of maize using Landsat data, IEEE Geosci. Remote S., 5, 133–137, 2008.
Gitelson, A. A., Peng, Y., Masek, J. G., Rundquist, D. C., Verma, S., Suyker, A., Baker, J. M., Hatfield, J. L., and Meyers, T.: Remote estimation of crop gross primary production with Landsat data, Remote Sens. Environ., 121, 404–414, doi:10.1016/j.rse.2012.02.017, 2012.
Goerner, A., Reichstein, M., Tomelleri, E., Hanan, N., Rambal, S., Papale, D., Dragoni, D., and Schmullius, C.: Remote sensing of ecosystem light use efficiency with MODIS-based PRI, Biogeosciences, 8, 189–202, doi:10.5194/bg-8-189-2011, 2011.
Hatfield, J. L., Gitelson, A. A., Schepers, J. S., and Walthall, C. L.: Application of spectral remote sensing for agronomic decisions, Agron. J., 100, 117–131, doi:10.2134/agronj2006.0370c, 2008.
Heinsch, F. A., Zhao, M. S., Running, S. W., Kimball, J. S., Nemani, R. R., Davis, K. J., Bolstad, P. V., Cook, B. D., Desai, A. R., Ricciuto, D. M., Law, B. E., Oechel, W. C., Kwon, H., Luo, H. Y., Wofsy, S. C., Dunn, A. L., Munger, J. W., Baldocchi, D. D., Xu, L. K., Hollinger, D. Y., Richardson, A. D., Stoy, P. C., Siqueira, M. B. S., Monson, R. K., Burns, S. P., and Flanagan, L. B.: Evaluation of remote sensing based terrestrial productivity from MODIS using regional tower eddy flux network observations, IEEE T. Geosci. Remote, 44, 1908–1925, 2006.
Hmimina, G., Dufrêne, E., and Soudani, K.: Relationship between photochemical reflectance index and leaf ecophysiological and biochemical parameters under two different water statuses: towards a rapid and efficient correction method using real-time measurements, Plant Cell Environ., 37, 473–487, 2014.
Inoue, Y., Peñuelas, J., Miyata, A., and Mano, M.: Normalized difference spectral indices for estimating photosynthetic efficiency and capacity at a canopy scale derived from hyperspectral and CO_2 flux measurements in rice, Remote Sens. Environ., 112, 156–172, 2008.
Jordan, C. F.: Derivation of leaf area index from quality of light on the forest floor, Ecology, 50, 663–666, 1969.
Kiniry, J. R., Burson, B. L., Evers, G. W., Williams, J. R., Sanchez, H., Wade, C., Featherston, J. W., and Greenwade, J.: Coastal bermudagrass, bahiagrass, and native range simulation for diverse sites in Texas, Agron. J., 99, 450–61, 2007.

BGD
11, 10323–10363, 2014

Title Page
Abstract | Introduction
Conclusions | References
Tables | Figures
◀◀ | ▶▶
◀ | ▶
Back | Close
Full Screen / Esc
Printer-friendly Version
Interactive Discussion

Meroni, M., Rossini, M., Guanter, L., Alonso, L., Rascher, U., Colombo, R., and Moreno, J.: Remote sensing of solar induced chlorophyll fluorescence: review of methods and applications, Remote Sens. Environ., 113, 2037–2051, 2009.
Monteith, J. L.: Solar radiation and productivity in tropical tcosystems, J. Appl. Ecol., 9, 747–766, 1972.
Monteith, J. L. and Moss, C. J.: Climate and the efficiency of crop production in Britain, Philos. T. Roy. Soc. B, 281, 277–294, doi:10.1098/rstb.1977.0140, 1977.
Nichol, C. J., Lloyd, J., Shibistova, O., Arneth, A., Roser, C., Knohl, A., Matsubara, S., and Grace, J.: Remote sensing of photosynthetic-light-use efficiency of a Siberian boreal forest, Tellus B, 54, 677–687, 2002.
Peng, Y., Gitelson, A. A., Keydan, G., Rundquist, D. C., and Moses, W.: Remote estimation of gross primary production in maize and support for a new paradigm based on total crop chlorophyll content, Remote Sens. Environ., 115, 978–989, 2011.
Peñuelas, J., Filella, I., Biel, C., Serrano, L., and Save, R.: The reflectance at the 950–970 nm region as an indicator of plant water status, Int. J. Remote Sens., 14, 1887–1905, 1993.
Peñuelas, J. and Filella, I.: Visible and near-infrared reflectance techniques for diagnosing plant physiological status, Trends Plant Sci., 3, 151–156, 1998.
Peñuelas, J., Gamon, J. A., Fredeen, A., Merino, J., and Field, C. B., Reflectance indices associated with physiological changes in nitrogen- and water-limited sunflower leaves, Remote Sens. Environ., 48, 135–146, 1994.
Peñuelas, J., Filella, I., and Gamon, J. A.: Assessment of photosynthetic radiation-use efficiency with spectral reflectance, New Phytol., 131, 291–296, 1995.
Polley, H. W., Phillips, B. L., Frank, A. B., Bradford, J. A., Sims, P. L., Morgan, J. A., and Kiniry, J. R.: Variability in light-use efficiency for gross primary productivity on Great Plains grasslands, Ecosystems, 14, 15–27, 2011.
Rahimzadeh-Bajgiran, P., Munehiro, M., and Omasa, K.: Relationships between the photochemical reflectance index (PRI) and chlorophyll fluorescence parameters and plant pigment indices at different leaf growth stages, Photosynt. Res., 113, 261–271, 2012.
Reichstein, M., Falge, E., Baldocchi, D., Papale, D., Valentini, R., Aubinet, M., Berbigier, P., Bernhofer, C., Buchmann, N., Gilmanov, T., Granier, A., Grünwald, T., Havrankova, K., Janous, D., Knohl, A., Laurela, T., Lohila, A., Loustau, D., Matteucci, G., Meyers, T., Miglietta, F., Ourcival, J.-M., Rambal, S., Rotenberg, E., Sanz, M., Seufert, G., Vaccari, F., Vesala, T., and Yakir, D.: On the separation of net ecosystem exchange into assimilation and

ecosystem respiration: review and improved algorithm, Glob. Change Biol., 11, 1424–1439, 2005.
Rossini, M., Meroni, M., Migliavacca, M., Manca, G., Cogliati, S., Busetto, L., Picchi, V., Cescatti, A., Seufert, G., and Colombo, R.: High resolution field spectroscopy measurements for estimating gross ecosystem production in a rice field, Agr. Forest Meteorol., 150, 1283–1296, 2010.
Rossini, M., Cogliati, S., Meroni, M., Migliavacca, M., Galvagno, M., Busetto, L., Cremonese, E., Julitta, T., Siniscalco, C., Morra di Cella, U., and Colombo, R.: Remote sensing-based estimation of gross primary production in a subalpine grassland, Biogeosciences, 9, 2565–2584, doi:10.5194/bg-9-2565-2012, 2012.
Rouse, J. W., Haas, R. H., Schell, J. A., and Deering, D. W.: Monitoring vegetation systems in the Great Plains with ERTS, 3rd ERTS Symposium, NASA SP-351 I, 1973.
Sakowska, K., Vescovo, L., Marcolla, B., Juszczak, R., Olejnik, J., and Gianelle, D.: Monitoring of carbon dioxide fluxes in a subalpine grassland ecosystem of the Italian Alps using a multispectral sensor, Biogeosciences Discuss., 11, 4729–4769, doi:10.5194/bgd-11-4729-2014, 2014.
Schwalm, C. R., Black, T. A., Amiro, B. D., Altaf Arain, M., Barr, A. G., Bourque, C. P. A., Dunn, A. L., Flanagan, L. B., Giasson, M. A., Lafleur, P. M., Margolis, H. A., McCaughey J. H., Orchansky, A. L., and Wofsy, S. C.: Photosynthetic light use efficiency of three biomes across an east–west continental-scale transect in Canada, Agr. Forest Meteorol., 140, 269–286, 2006.
Soudani, K., Hmimina, G., Dufrêne, E., Berveiller, D., Delpierre, N., Ourcival, J.-M., Rambal, S., and Joffre, R.: Relationships between photochemical reflectance index and light-use efficiency in deciduous and evergreen broadleaf forests, Remote Sens. Environ., 144, 73–84, 2014.
Soussana, J. F., Allard, V., Pilegaard, K., Ambus, C., Campbell, C., Ceschia, E., Clifton-Brown, J., Czobel, S., Domingues, R., Flechard, C., Fuhrer, J., Hensen, A., Horvath, L., Jones, M., Kasper, G., Martin, C., Nagy, Z., Neftel, A., Raschi, A., Baronti, S., Rees, R. M., Skiba, U., Stefani, P., Manca, G., Sutton, M., Tuba, Z., and Valentini, R.: Full accounting of the greenhouse gas (CO_2, N_2O, CH_4) budget of nine European grassland sites, Agr. Ecol. Environ., 121, 121–134, 2007.
Vescovo, L., Wohlfahrt, G., Balzarolo, M., Pilloni, S., Sottocornola, M., Rodeghiero, M., and Gianelle, D.: New spectral vegetation indices based on the near-infrared shoulder wavelenghts

fro remote sensign detection of grassland phytomass, Int. J. Remote Sens., 33, 2178–2195, 2012.
Wohlfahrt, G., Sapinsky, S., Tappeiner, U., and Cernusca, A.: Estimation of plant area index of grasslands from measurements of canopy radiation profiles, Agr. Forest Meteorol., 109, 1–12, 2001.
Wohlfahrt, G., Anderson-Dunn, M., Bahn, M., Balzarolo, M., Berninger, F., Campbell, C., Carrara, A., Cescatti, A., Christensen, T., Dore, S., Eugster, W., Friborg, T., Furger, M., Gianelle, D., Gimeno, C., Hargreaves, K., Hari, P., Haslwanter, A., Johansson, T., Marcolla, B., Milford, C., Nagy, Z., Nemitz, E., Rogiers, N., Sanz, M. J., Siegwolf, R. T. W., Susiluoto, S., Sutton, M., Tuba, Z., Ugolini, F., Valentini, R., Zorer, R., and Cernusca, A.: Biotic, abiotic and management controls on the net ecosystem CO_2 exchange of European mountain grasslands, Ecosystems, 11, 1338–1351, 2008.
Wohlfahrt, G., Pilloni, S., Hörtnagl, L., and Hammerle, A.: Estimating carbon dioxide fluxes from temperate mountain grasslands using broad-band vegetation indices, Biogeosciences, 7, 683–694, doi:10.5194/bg-7-683-2010, 2010.

BGD
11, 10323–10363, 2014

Relationship between hyperspectral reflectance and CO_2 exchange

M. Balzarolo et al.

Table 1. Description of the study sites and period.

Site characteristics	Amplero (IT-Amp)	Neustift (AT-Neu)	Monte Bondone (IT-MBo)
Latitude	41.9041	47.1162	46.0296
Longitude	13.6052	11.3204	11.0829
Elevation (m)	884	970	1550
Mean annual temperature (°C)	10.0	6.5	5.5
Mean annual precipitation (mm)	1365	852	1189
Vegetation type	Seslerietum apenninae	Pastinaco – Arrhenatheretum	Nardetum Alpigenum
Study period[1]	111–170, 2006 (9)	122–303, 2006 (16)	129–201, 2005 (13) 124–192, 2006 (12)

[1] from-to DOY, year (number of hyperspectral measurement dates)

BGD
11, 10323–10363, 2014

Relationship between hyperspectral reflectance and CO_2 exchange

M. Balzarolo et al.

Table 2. Summary of the vegetation indices characteristics used in this study.

Index name and acronym	Formula	Use	Reference
Simple Spectral Ratio Indices			
Simple Ratio (SR or RVI)	$SR = R_{830}/R_{660}$	Greenness	Jordan (1969)
Green Ratio Index (GRI)	$\mathrm{GRI} = R_{830}/R_{550}$	Greenness	Peñuelas and Filella (1998)
Water Index (WI)	$\mathrm{WI} = R_{900}/R_{970}$	Water content, leaf water potential, canopy water content	Peñuelas et al. (1993)
Simple Ratio Pigment Index (SRPI)	$\mathrm{SRPI} = (R_{430})/(R_{680})$		Peñuelas et al. (1995)
Normalized Spectral Difference Vegetation Indices			
Normalized Difference Vegetation Index (NDVI)	$\mathrm{NDVI} = (R_{830} - R_{660})/(R_{830} + R_{660})$	Greenness	Rouse et al. (1973)
Normalized Phaeophytinization Index (NPQI)	$\mathrm{NPQI} = (R_{415} - R_{435})/(R_{415} + R_{435})$	Carotenoid/Chlorophyll ratio	Barnes et al. (1992)
Normalized Pigment Chlorophyll Index (NPCI)	$\mathrm{NPCI} = (R_{680} - R_{430})/(R_{680} + R_{430})$	Chlorophyll ratio	Peñuelas et al. (1994)
Chlorophyll Index (CI)	$\mathrm{CI} = (R_{750} - R_{705})/(R_{750} + R_{705})$	Chlorophyll content	Gitelson and Merzlyak (1997)
Structural Independent Pigment Index (SIPI)	$\mathrm{SIPI} = (R_{800} - R_{445})/(R_{800} + R_{445})$	Chlorophyll content	Peñuelas et al. (1995)
Photochemical Reflectance Index (PRI)	$\mathrm{PRI} = (R_{531} - R_{570})/(R_{531} + R_{570})$	Photosynthetic light use efficiency (and leaf pigment contents)	Gamon et al. (1992)
Improved for soil and atmospheric effects			
Enhanced Vegetation Index (EVI)	$\mathrm{EVI} = 2.5(R_{830} - R_{660})/(1 + R_{830} + 6R_{660} - 7.5R_{460})$	Vegetation Index improved for soil and atmospheric effects	Huete et al. (1997)

BGD
11, 10323–10363, 2014

Table 3. Results of statistic of linear and exponential regression models between VIs and eco-physiological parameters: α, ε (midday average) and GPP_{max}. R^2 – Coefficient of determination; RMSE – Root Mean Square Error; and AIC – Akaike information criterion. Bold letters indicate the best model between linear and exponential models. Italic letters highlight the model with the lowest AIC.

	α												ε											
	Amplero			Neustift			Monte Bondone			All			Amplero			Neustift			Monte Bondone			All		
	R^2	RMSE	AIC	R^2	RMSE	AIC	R^2	RMSE	AIC	R^2	RMSE	AIC	R^2	RMSE	AIC	R^2	RMSE	AIC	R^2	RMSE	AIC	R^2	RMSE	AIC
VI	–	$\frac{\mu mol_{CO_2}}{\mu mol_{phot}}$	–	–	$\frac{\mu mol_{CO_2}}{\mu mol_{phot}}$	–	–	$\frac{\mu mol_{CO_2}}{\mu mol_{phot}}$	–	–	$\frac{\mu mol_{CO_2}}{\mu mol_{phot}}$	–	–	$\frac{\mu mol_{CO_2}}{\mu mol_{phot}}$	–	–	$\frac{\mu mol_{CO_2}}{\mu mol_{phot}}$	–	–	$\frac{\mu mol_{CO_2}}{\mu mol_{phot}}$	–	–	$\frac{\mu mol_{CO_2}}{\mu mol_{phot}}$	–
Linear model																								
SR	0.7	0.0	−72	0.0	0.1	−35	0.3	0.0	−160	0.0	0.1	−156	**0.6**	**0.0**	**−61**	0.3	0.0	−54	0.3	0.0	−86	0.2	0.0	−186
GRI	0.5	0.0	−67	0.0	0.1	−35	0.2	0.0	−157	0.0	0.1	−157	0.3	0.0	−57	**0.5**	**0.0**	**−59**	0.5	0.0	−90	**0.5**	**0.0**	**−196**
WI	0.7	0.0	−71	0.3	0.1	−40	0.2	0.0	−155	0.0	0.1	−157	0.5	0.0	−60	0.2	0.0	−52	0.3	0.0	−86	0.2	0.0	−187
NDVI	0.7	0.0	−73	0.0	0.1	−35	**0.3**	**0.0**	**−161**	0.0	0.1	−157	0.4	0.0	−58	0.4	0.0	−55	0.6	0.0	−96	0.4	0.0	−194
SIPI	0.7	0.0	−73	0.0	0.1	−36	0.3	0.0	−160	0.1	0.1	−159	0.3	0.0	−56	0.3	0.0	−54	**0.7**	**0.0**	**−103**	0.4	0.0	−193
CI	0.7	0.0	−73	0.0	0.1	−35	0.3	0.0	−161	0.0	0.1	−156	0.4	0.0	−58	0.4	0.0	−56	0.5	0.0	−92	0.4	0.0	−192
PRI	*0.8*	*0.0*	*−76*	0.0	0.1	−36	0.3	0.0	−159	0.2	0.0	−170	0.6	0.0	−61	0.1	0.0	−49	0.0	0.1	−76	0.0	0.0	−176
EVI	0.8	0.0	*−75*	0.0	0.1	−35	0.3	0.0	−159	0.0	0.1	−157	0.4	0.0	−58	0.4	0.0	−56	0.5	0.0	−94	0.4	0.0	−192
NPQI	0.4	0.0	−66	**0.4**	**0.1**	**−43**	0.0	0.0	−151	*0.4*	*0.0*	*−177*	0.0	0.0	−53	0.0	0.1	−48	0.3	0.0	−83	0.1	0.0	−183
NPCI	0.7	0.0	−72	0.1	0.1	−36	0.3	0.0	−158	0.3	0.0	−175	0.3	0.0	−56	0.2	0.0	−51	0.0	0.1	−76	0.0	0.0	−176
SRPI	0.6	0.0	−71	0.1	0.1	−36	0.3	0.0	−158	0.3	0.0	−176	0.2	0.0	−56	0.2	0.0	−51	0.0	0.1	−76	0.0	0.0	−176
Exponential model																								
SR	0.7	0.0	−71	0.0	0.1	−35	0.3	0.0	−159	0.0	0.1	−156	*0.8*	*0.0*	*−68*	0.4	0.0	−55	0.5	0.0	−91	0.2	0.0	−189
GRI	0.5	0.0	−67	0.0	0.1	−35	0.2	0.0	−157	0.0	0.1	−157	0.3	0.0	−57	*0.5*	*0.0*	*−58*	0.6	0.0	−97	*0.5*	*0.0*	*−211*
WI	0.6	0.0	−70	0.2	0.1	−40	0.2	0.0	−155	0.0	0.1	−157	0.6	0.0	−61	0.2	0.0	−50	0.5	0.0	−93	0.2	0.0	−191
NDVI	0.7	0.0	−73	0.0	0.1	−35	0.3	0.0	−161	0.0	0.1	−157	0.7	0.0	−64	0.3	0.0	−54	0.7	0.0	−107	0.4	0.0	−205
SIPI	0.8	0.0	−75	0.0	0.1	−36	*0.3*	*0.0*	*−161*	0.1	0.1	−160	0.5	0.0	−59	0.3	0.0	−53	*0.8*	*0.0*	*−114*	0.4	0.0	−203
CI	0.7	0.0	−72	0.0	0.1	−35	0.3	0.0	−161	0.0	0.1	−156	0.6	0.0	−62	0.4	0.0	−55	0.7	0.0	−103	0.4	0.0	−201
PRI	0.8	0.0	−74	0.0	0.1	−36	0.3	0.0	−159	0.2	0.0	−170	0.8	0.0	−67	0.1	0.0	−50	0.0	0.1	−76	0.0	0.0	−176
EVI	**0.8**	**0.0**	**−76**	0.0	0.1	−35	0.3	0.0	−159	0.0	0.1	−157	0.6	0.0	−62	0.4	0.0	−56	0.7	0.0	−103	0.4	0.0	−200
NPQI	0.3	0.0	−65	*0.4*	*0.1*	*−43*	0.0	0.0	−151	**0.4**	**0.0**	**−184**	0.0	0.0	−53	0.0	0.1	−48	0.4	0.0	−88	0.1	0.0	−182
NPCI	0.6	0.0	−70	0.1	0.1	−36	0.3	0.0	−158	0.3	0.0	−176	0.2	0.0	−56	0.2	0.0	−52	0.0	0.1	−76	0.0	0.0	−176
SRPI	0.5	0.0	−68	0.1	0.1	−36	0.3	0.0	−158	0.3	0.0	−175	0.2	0.0	−56	0.2	0.0	−52	0.0	0.1	−76	0.0	0.0	−176

BGD
11, 10323–10363, 2014

BGD

11, 10323–10363, 2014

Table 3. Continued.

	GPP$_{max}$											
	Amplero			Neustift			Monte Bondone			All		
	R^2	RMSE	AIC	R^2	RMSE	AIC	R^2	RMSE	AIC			
VI	–	$\frac{\mu mol_{CO_2}}{m^2 s}$	–	–	$\frac{\mu mol_{CO_2}}{m^2 s}$	–	–	$\frac{\mu mol_{CO_2}}{m^2 s}$	–	–	$\frac{\mu mol_{CO_2}}{m^2 s}$	–
Linear model												
SR	*0.9*	*1.1*	*30*	0.1	7.3	111	0.4	4.8	151	0.2	6.5	356
GRI	0.8	2.0	40	0.1	7.1	110	0.3	5.2	155	0.1	6.9	364
WI	0.9	1.4	34	0.0	7.6	112	0.3	5.2	155	0.1	7.0	364
NDVI	0.9	1.4	33	0.1	7.0	110	0.4	4.7	150	0.2	6.3	354
SIPI	0.8	1.9	39	0.2	6.6	108	0.4	4.6	149	**0.3**	**6.1**	**351**
CI	0.9	1.5	35	0.2	6.8	109	**0.5**	**4.5**	**148**	0.2	6.4	354
PRI	0.8	2.0	40	0.3	6.3	106	0.3	5.3	156	0.2	6.4	354
EVI	0.9	1.4	33	0.1	7.2	111	0.4	4.7	151	0.2	6.6	357
NPQI	0.3	3.8	51	0.2	6.9	109	0.1	5.9	162	0.0	7.2	368
NPCI	0.6	2.8	46	*0.4*	*6.1*	*105*	0.3	5.2	155	0.2	6.5	355
SRPI	0.6	2.9	47	0.3	6.2	106	0.3	5.2	155	0.2	6.6	357
Exponential model												
SR	0.9	1.5	34	0.1	7.3	111	0.4	4.9	152	0.2	6.5	358
GRI	0.7	2.3	43	0.1	7.2	110	0.3	5.3	156	0.1	6.9	364
WI	0.8	1.8	38	0.0	7.6	112	0.3	5.3	157	0.1	7.0	365
NDVI	**0.9**	**1.2**	**31**	0.1	7.1	110	0.4	4.7	150	0.2	6.3	354
SIPI	0.9	1.7	37	0.2	6.7	108	0.5	4.5	148	*0.3*	*6.1*	*350*
CI	0.9	1.5	35	0.2	6.9	109	*0.5*	*4.5*	*148*	0.2	6.4	356
PRI	0.8	2.0	40	0.3	6.5	107	0.3	5.3	156	0.2	6.4	356
EVI	0.9	1.2	31	0.1	7.3	111	0.4	4.8	152	0.2	6.6	359
NPQI	0.2	3.9	52	0.1	7.1	110	0.1	5.9	162	0.0	7.2	368
NPCI	0.5	3.2	48	**0.3**	**6.4**	**107**	0.3	5.3	156	0.2	6.5	357
SRPI	0.4	3.4	49	0.3	6.5	108	0.3	5.3	157	0.2	6.6	359

Table 4. Results of statistic of linear and exponential regression models between VIs and midday average CO_2 fluxes: NEE and GPP. R^2 – Coefficient of determination; RMSE – Root Mean Square Error; and AIC – Akaike information criterion. Bold letters indicate the best model between linear and exponential models. Italic letters highlight the model with the lowest AIC.

	GPP											
	Amplero			Neustift			Monte Bondone			All		
	R^2	RMSE	AIC	R^2	RMSE	AIC	R^2	RMSE	AIC	R^2	RMSE	AIC
VI	–	$\frac{\mu mol_{CO_2}}{m^2 s}$	–	–	$\frac{\mu mol_{CO_2}}{m^2 s}$	–	–	$\frac{\mu mol_{CO_2}}{m^2 s}$	–	–	$\frac{\mu mol_{CO_2}}{m^2 s}$	–
Linear model												
SR	0.6	2.8	46	0.2	9.0	118	0.5	4.4	147	0.2	7.2	368
GRI	0.5	3.0	48	0.2	8.9	117	0.5	4.5	148	0.1	7.9	377
WI	**0.7**	**2.4**	**43**	0.1	9.3	119	0.4	4.9	153	0.1	7.6	374
NDVI	0.5	3.2	49	0.2	9.0	118	0.5	4.4	146	0.2	7.1	367
SIPI	0.3	3.7	51	0.2	8.8	117	0.5	4.5	148	0.3	6.7	365
CI	0.5	3.1	48	0.3	8.4	116	**0.6**	**4.1**	**144**	0.2	7.2	367
PRI	0.4	3.5	50	0.3	8.2	115	0.2	5.4	157	*0.3*	*6.8*	*361*
EVI	0.4	3.4	50	0.2	8.9	117	0.5	4.4	147	0.2	7.1	367
NPQI	0.1	4.4	54	0.1	9.3	119	0.1	5.7	160	0.1	7.8	377
NPCI	0.1	4.3	54	*0.4*	*8.0*	*114*	0.2	5.4	157	0.3	6.9	362
SRPI	0.1	4.4	54	0.4	8.0	114	0.2	5.4	157	0.3	7.0	363
Exponential model												
SR	0.7	2.5	44	0.1	9.0	118	0.5	4.5	149	0.2	7.2	369
GRI	0.6	2.9	47	0.2	8.9	117	0.4	4.6	149	0.1	7.9	378
WI	*0.8*	*1.9*	*40*	0.0	9.4	119	0.3	5.1	154	0.1	7.6	375
NDVI	0.6	3.0	47	0.2	9.0	118	0.5	4.3	146	0.2	7.1	366
SIPI	0.4	3.6	51	0.2	8.7	117	0.5	4.2	145	**0.3**	**6.7**	**361**
CI	0.6	3.0	47	0.3	8.4	116	*0.6*	*4.0*	*142*	0.2	7.2	369
PRI	0.4	3.5	50	**0.3**	**8.1**	**114**	0.2	5.4	157	0.3	6.8	362
EVI	0.4	3.4	49	0.2	9.0	118	0.5	4.5	148	0.2	7.1	367
NPQI	0.1	4.4	54	0.1	9.4	119	0.1	5.8	161	0.1	7.8	377
NPCI	0.1	4.3	54	0.4	8.1	115	0.2	5.4	158	0.3	6.9	364
SRPI	0.0	4.4	54	0.3	8.3	115	0.2	5.4	158	0.3	7.0	365

BGD
11, 10323–10363, 2014

Table 4. Continued.

	NEE											
	Amplero			Neustift			Monte Bondone			All		
	R^2	RMSE	AIC	R^2	RMSE	AIC	R^2	RMSE	AIC	R^2	RMSE	AIC
VI	–	$\frac{\mu mol_{CO_2}}{m^2 s}$	–	–	$\frac{\mu mol_{CO_2}}{m^2 s}$	–	–	$\frac{\mu mol_{CO_2}}{m^2 s}$	–	–	$\frac{\mu mol_{CO_2}}{m^2 s}$	–
Linear model												
SR	0.7	2.4	43	0.2	8.2	115	0.4	4.2	145	0.2	6.2	352
GRI	0.7	2.5	44	0.2	8.1	114	0.4	4.4	147	0.1	6.7	360
WI	**0.8**	**1.9**	**39**	0.1	8.7	117	0.3	4.6	150	0.1	6.6	358
NDVI	0.6	2.8	46	0.2	8.1	114	0.4	4.2	145	0.3	6.1	351
SIPI	0.4	3.3	49	0.2	7.8	113	0.4	4.2	145	0.3	5.9	350
CI	0.6	2.7	46	0.3	7.6	112	**0.5**	**3.9**	**141**	**0.2**	**6.2**	**350**
PRI	0.5	3.3	49	0.3	7.4	112	0.2	5.1	154	0.2	6.3	354
EVI	0.5	3.1	48	0.2	8.1	114	0.4	4.2	145	0.2	6.3	353
NPQI	0.1	4.3	54	0.1	8.3	115	0.1	5.3	156	0.0	7.0	365
NPCI	0.2	4.1	53	*0.4*	*6.8*	*109*	0.3	4.8	152	0.2	6.3	353
SRPI	0.1	4.2	53	0.4	6.9	109	0.3	4.8	152	0.2	6.4	354
Exponential model												
SR	0.8	2.0	40	0.1	8.2	115	0.4	4.3	146	0.2	6.2	353
GRI	0.7	2.3	43	0.2	8.2	115	0.4	4.5	148	0.1	6.7	361
WI	*0.9*	*1.6*	*36*	0.0	8.7	117	0.3	4.8	151	0.1	6.6	359
NDVI	0.7	2.5	44	0.2	8.1	114	0.5	4.2	144	0.3	6.1	351
SIPI	0.5	3.3	49	0.2	7.7	113	0.5	4.0	142	*0.3*	*5.9*	*348*
CI	0.7	2.4	44	0.3	7.6	112	*0.5*	*3.8*	*140*	0.2	6.2	352
PRI	0.5	3.3	49	0.3	7.4	112	0.2	5.1	154	0.2	6.3	355
EVI	0.5	3.0	48	0.2	8.2	115	0.4	4.2	145	0.2	6.3	354
NPQI	0.1	4.3	54	0.1	8.5	116	0.1	5.3	156	0.0	7.0	365
NPCI	0.1	4.2	53	**0.4**	**7.2**	**111**	0.3	4.8	152	0.2	6.3	355
SRPI	0.1	4.3	54	0.3	7.3	111	0.3	4.9	152	0.2	6.4	355

BGD

11, 10323–10363, 2014

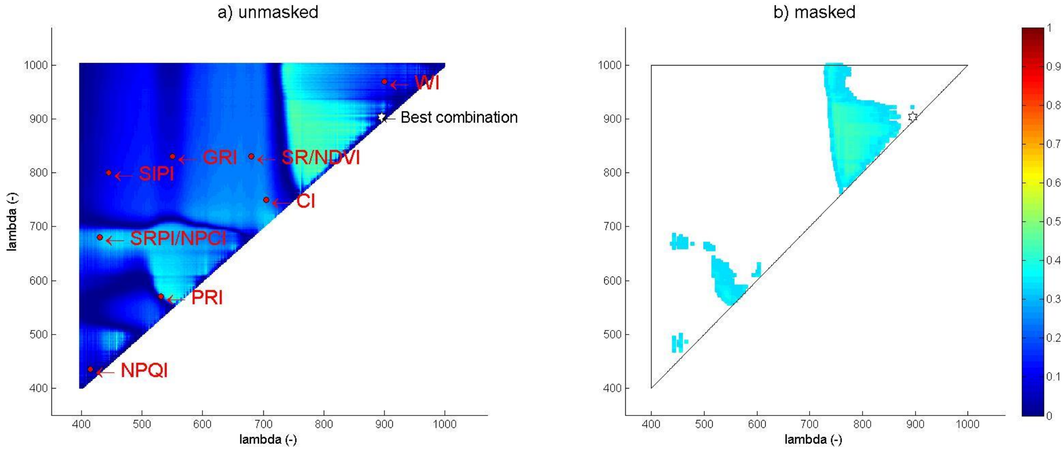

Figure 1. A selected example of a correlogram between NSD-type indices and midday average GPP for all sites pooled. Plot in **(a)** shows all R^2 values (unmasked), the asterisk symbol indicates the two-band combination with the highest R^2 value and the dots indicate the location of the reference VIs reported in Table 2. Plot in **(b)** is the same as in **(a)** but shows only the highest 10 % of the R^2 values with all other values masked.

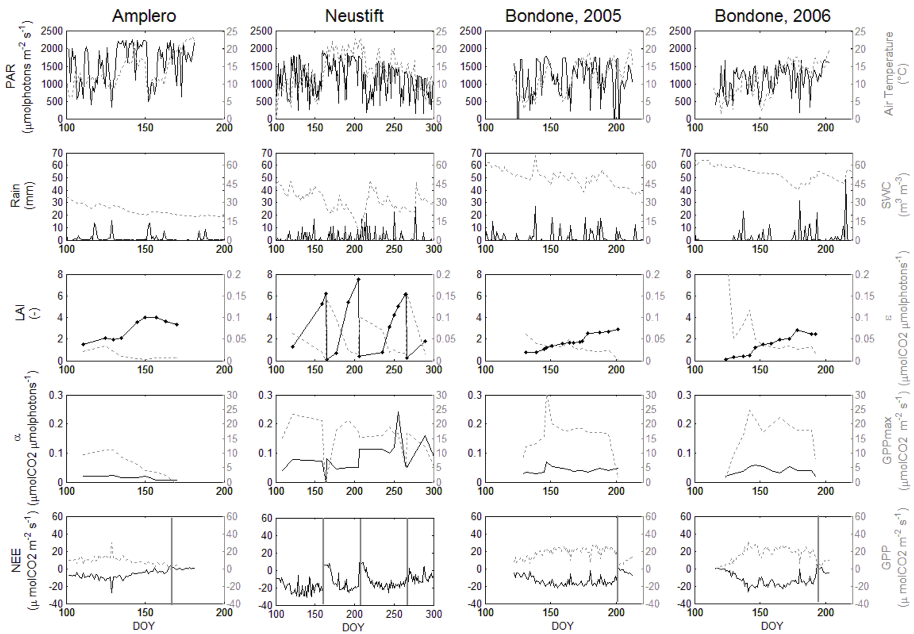

Figure 2. Seasonal variation of meteorological variables, LAI, CO_2 fluxes and ecophysiological parameters for the period of the hyperspectral measurements at the three investigated grasslands. **(a)** Midday average photosynthetically active radiation (PAR; $\mu mol\,m^{-2}\,s^{-1}$; solid black line) and daily average air temperature (°C; dotted grey line); **(b)** daily precipitation (Rain; mm; solid black line) and daily average soil water content (SWC; $m^3\,m^{-3}$; dotted grey line); **(c)** Leaf Area Index (LAI; $m^2\,m^{-2}$; solid black line) and light use efficiency (ε; $\mu mol\,photons\,\mu mol\,CO_2^{-1}$; dotted grey line); **(d)** apparent quantum yield (α; $\mu mol\,CO_2\,\mu mol\,photons^{-1}$; solid black line) and gross primary production at saturating light (GPP_{max}; $\mu mol\,m^{-2}\,s^{-1}$; dotted grey line); **(e)** midday average net ecosystem CO_2 exchange (NEE; $\mu mol\,m^{-2}\,s^{-1}$; solid black line) and gross primary production (GPP; $\mu mol\,m^{-2}\,s^{-1}$; grey dotted line); vertical lines in the lowermost panels indicate the dates of mowing.

BGD

11, 10323–10363, 2014

Relationship between hyperspectral reflectance and CO_2 exchange

M. Balzarolo et al.

Title Page
Abstract | Introduction
Conclusions | References
Tables | Figures
◀| |▶
◀ ▶
Back | Close
Full Screen / Esc
Printer-friendly Version
Interactive Discussion

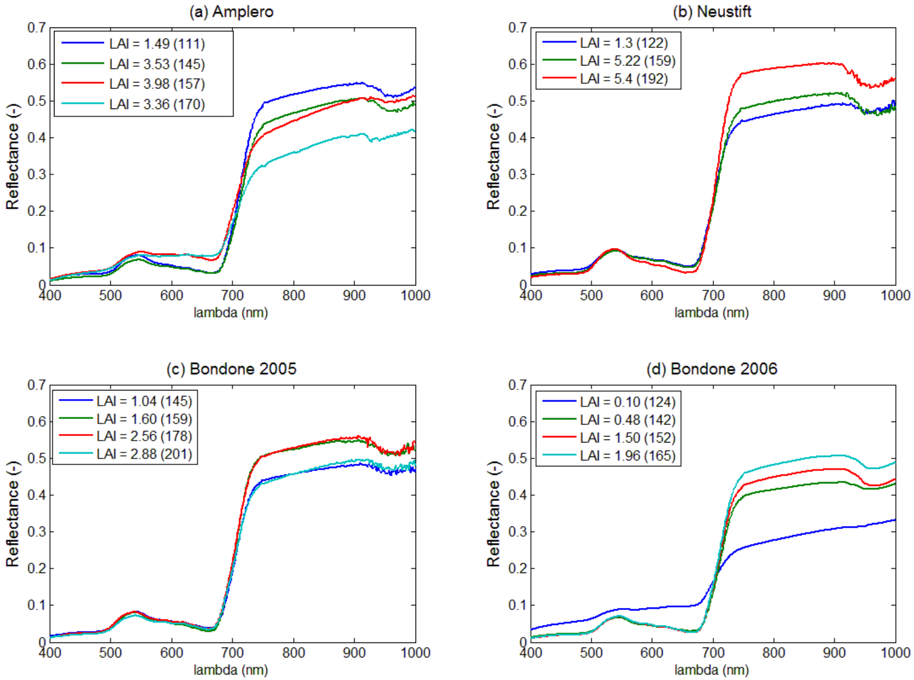

Figure 3. Selected grassland spectral signatures during the growing seasons. The figure legends indicates the corresponding leaf area index (LAI; $m^2\,m^{-2}$) and the day of year (in parenthesis).

BGD
11, 10323–10363, 2014

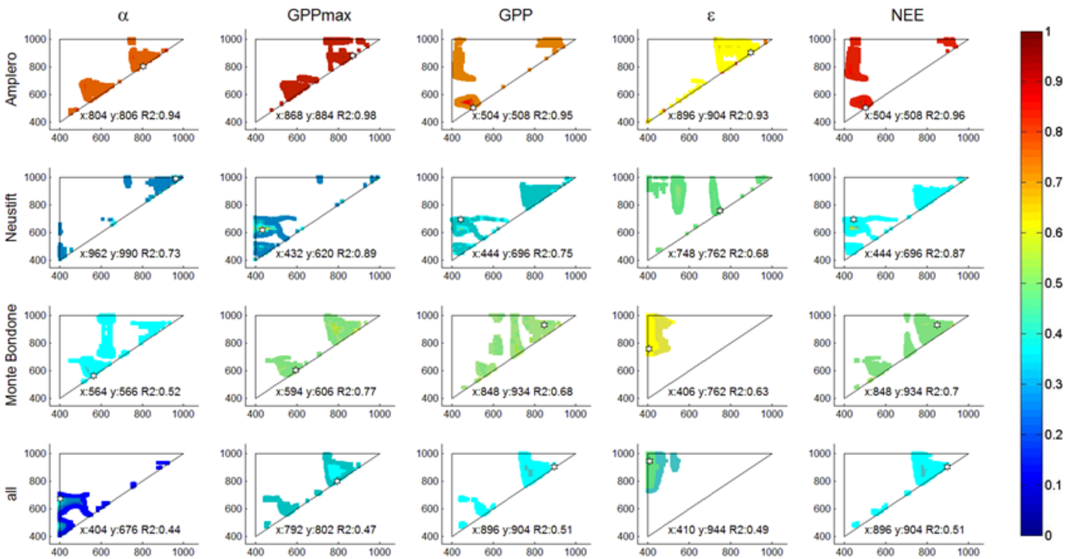

Figure 4. Correlograms of the highest 10 % of the R^2 values for α, GPP_{max} and midday averaged GPP, ε and NEE and NSD-type indices for Amplero, Neustift, Monte Bondone (both study years pooled) and all sites pooled for the linear model. The asterisks indicate the position of paired band combinations corresponding to the maximum R^2. The unmasked correlograms are shown in the Supplement (Fig. S1).

BGD

11, 10323–10363, 2014

Relationship between hyperspectral reflectance and CO_2 exchange

M. Balzarolo et al.

Title Page
Abstract | Introduction
Conclusions | References
Tables | Figures
◀| |▶
◀ ▶
Back | Close
Full Screen / Esc
Printer-friendly Version
Interactive Discussion

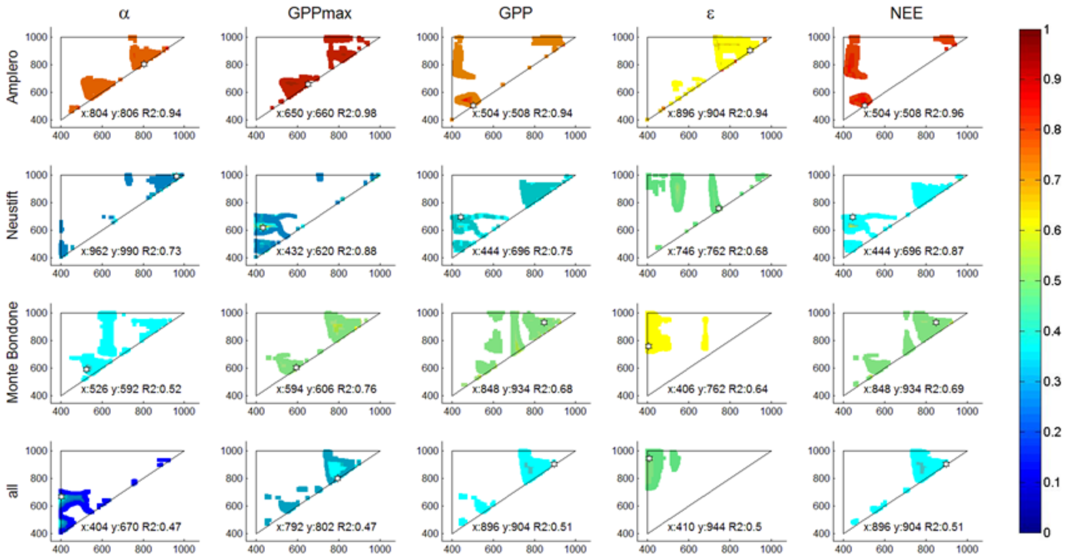

Figure 5. Correlograms of the highest 10 % of the R^2 values for α, GPP_{max} and midday averaged GPP, ε and NEE and SR-type indices for Amplero, Neustift, Monte Bondone (both study years pooled) and all sites pooled for the linear model. The asterisks indicate the position of paired band combinations corresponding to the maximum R^2. The unmasked correlograms are shown in the Supplement (Fig. S2).

BGD

11, 10323–10363, 2014

Relationship between hyperspectral reflectance and CO_2 exchange

M. Balzarolo et al.

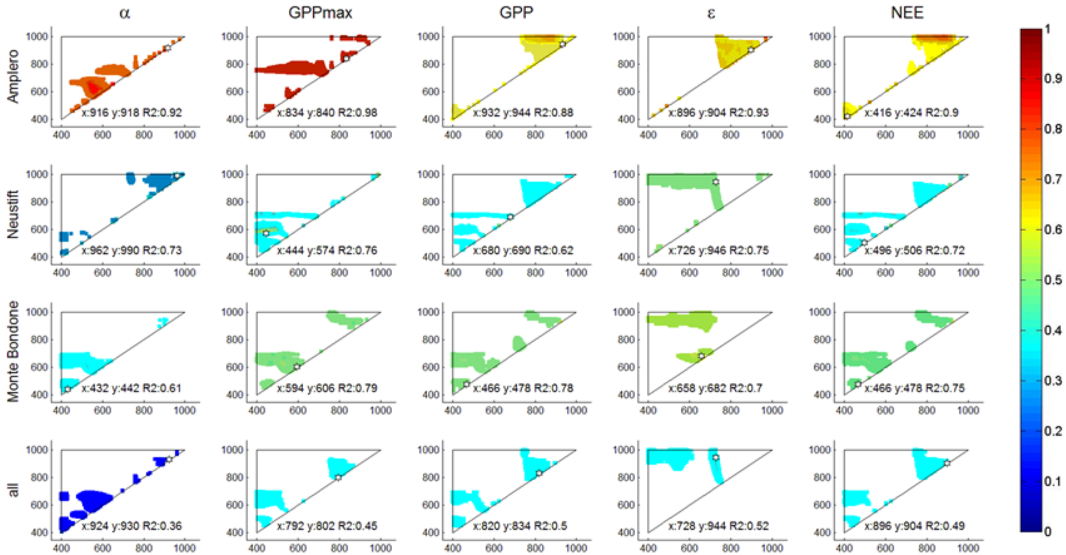

Figure 6. Correlograms of the highest 10 % of the R^2 values for α, GPP_{max} and midday averaged GPP, ε and NEE and SD-type indices for Amplero, Neustift, Monte Bondone (both study years pooled) and all sites pooled for the linear model. The asterisks indicate the position of paired band combinations corresponding to the maximum R^2. The unmasked correlograms are shown in the Supplement (Fig. S3).

BGD
11, 10323–10363, 2014

Relationship between hyperspectral reflectance and CO_2 exchange

M. Balzarolo et al.

Title Page
Abstract Introduction
Conclusions References
Tables Figures
◀◀ ▶▶
◀ ▶
Back Close
Full Screen / Esc
Printer-friendly Version
Interactive Discussion

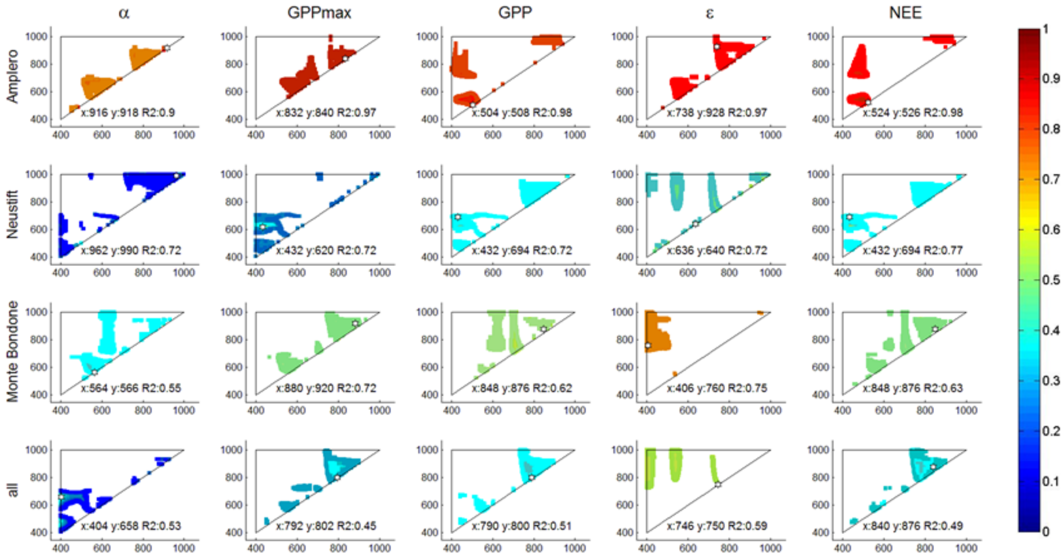

Figure 7. Correlograms of the highest 10 % of the R^2 values for α, GPP_{max} and midday averaged GPP, ε and NEE and NSD-type indices for Amplero, Neustift, Monte Bondone (both study years pooled) and all sites pooled for the exponential model. The asterisks indicate the position of paired band combinations corresponding to the maximum R^2. The unmasked correlograms are shown in the Supplement (Fig. S7).

BGD
11, 10323–10363, 2014

Relationship between hyperspectral reflectance and CO_2 exchange

M. Balzarolo et al.

Title Page
Abstract | Introduction
Conclusions | References
Tables | Figures
◀| |▶
◀ ▶
Back | Close
Full Screen / Esc
Printer-friendly Version
Interactive Discussion

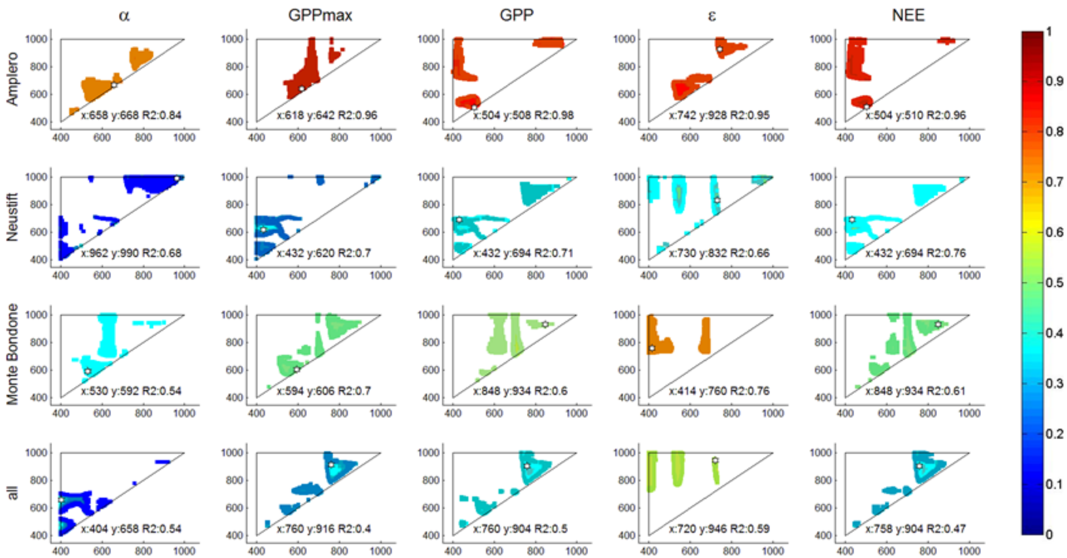

Figure 8. Correlograms of the highest 10 % of the R^2 values for α, GPP_{max} and midday averaged GPP, ε and NEE and SR-type indices for Amplero, Neustift, Monte Bondone (both study years pooled) and all sites pooled for the exponential model. The asterisks indicate the position of paired band combinations corresponding to maximum R^2. The unmasked correlograms are shown in the Supplement (Fig. S8).

BGD
11, 10323–10363, 2014

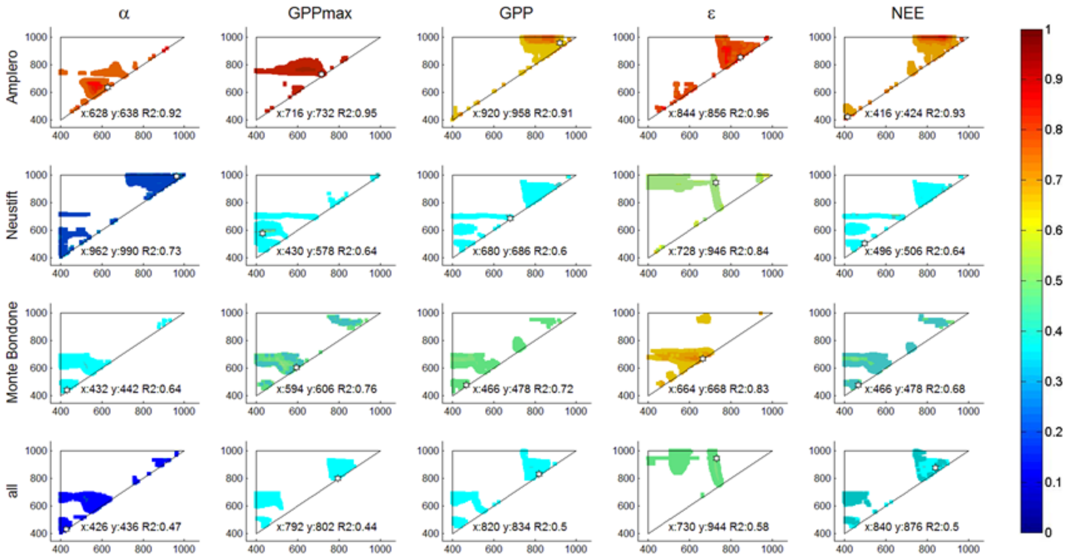

Figure 9. Correlograms of the highest 10 % of the R^2 values for α, GPP_{max} and midday averaged GPP, ε and NEE and SD-type indices for Amplero, Neustift, Monte Bondone (both study years pooled) and all sites pooled for the exponential model. The asterisks indicate the position of paired band combinations corresponding to maximum R^2. The unmasked correlograms are shown in the Supplement (Fig. S9).

BGD
11, 10323–10363, 2014

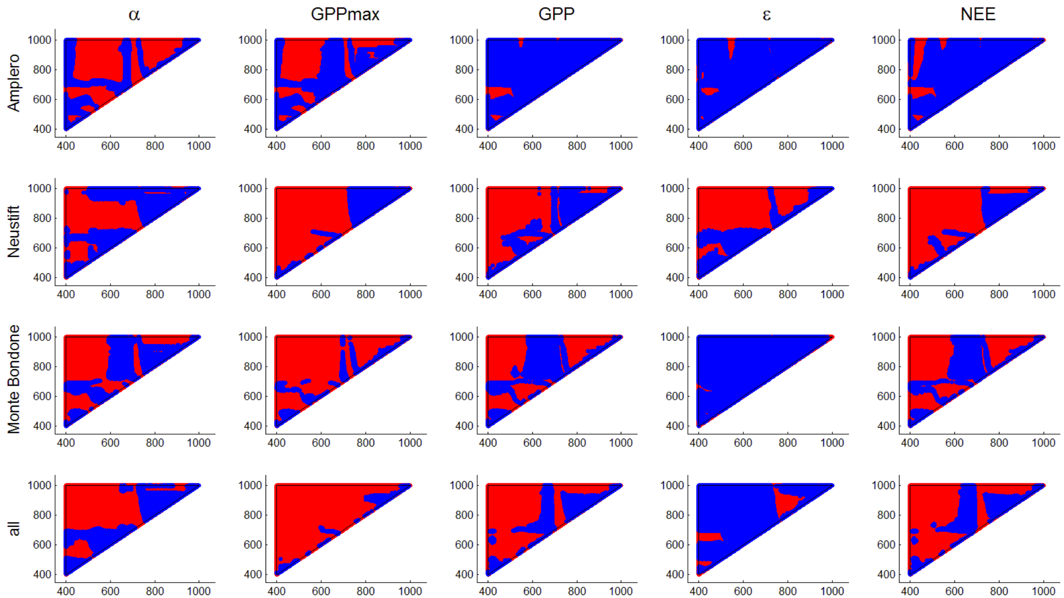

Figure 10. Correlograms of the differences between AIC (Akaike information criterion) obtained for linear and exponential models for α, GPP_{max} and midday averaged GPP, ε and NEE and NSD-type indices for Amplero, Neustift, Monte Bondone (both study years pooled) and all sites pooled. Red areas indicate waveband combinations where the linear model performed better than exponential one, while blue areas indicate the reverse.